Locally variable turbulent Prandtl number considerations on the modeling of Liquid Rocket Engines operating above the critical point

Leandro Magalhães, André Silva*, Jorge Barata
*AEROG - LAETA, University of Beira Interior, Covilhã, Portugal
*Corresponding author: andre@ubi.pt

Abstract
The general idea behind the present work is to study the injection of a cryogenic liquid numerically into rocket engines, where propellant conditions are above the thermodynamic critical point, for a non-reactive case.
The singular behavior of thermodynamic and transport properties at and around the critical point makes this a most challenging task. While mass diffusivity, surface tension, and latent heat are zero at the critical point, isentropic compressibility, specific heat, and thermal conductivity tend to infinity. As a result, the distinction between liquid and solid phases disappears. Ultimately, the fluid has liquid-like density and gas-like properties, mass diffusion replaces vaporization as a governing parameter, and it dominates over jet atomization. Henceforth, any model used incorporates as close as possible to reality, the variation of thermodynamic and transport properties.
An incompressible variable-density flow is simulated using Favre averages (FANS) with a locally variable turbulent Prandtl number, taking into account the potential core, transition, and the self-similar region of the jet. The use of a turbulence model with a variable turbulent Prandtl number arises from the ineffectiveness in predicting observed anisotropies in the thermal eddy diffusivity fields when this value is taken as a constant.
Favre averaged conservation equations for mass, momentum, and energy are coupled with the κ-ϵ two-equation turbulence model and discretized following the third order upwind QUICK scheme. Stability and accuracy of the results are maintained through a careful selection of the parameters involved in the models. The use of the conservation equation for energy is justified as an indirect means to evaluate the thermal field. Results are compared with experimental cases for validation purposes as well as LES computations for performance comparison and evaluation of the degree of model complexity needed to achieve satisfactory results.

Keywords
supercritical fluids, variable turbulent Prandtl number, cryogenics

Introduction
Increase in both pressure and temperature of fuels and/or oxidizers in Liquid Rocket Engines (LRE), while enhancing fuel efficiency, leads to an increase in phenomena complexity. As the thermodynamic singularity which is the critical point is approached, some concepts regarded as universal lose their ground in favor of an entirely new analysis. While mass diffusivity, surface tension, and latent heat are zero at the critical point, isentropic compressibility, specific heat, and thermal conductivity tend to infinity. The ruling over jet atomization sees mass diffusion replacing vaporization.
Turbulence models are still relying on the concepts of eddy diffusivity of momentum and turbulent Prandtl number [1]. While an increase in turbulence model complexity could contribute to marginal improvements in terms of accuracy, they would come at a tremendous computational cost. This resulted in the use of a constant turbulent Prandtl number in simulations (typically 0.85-0.9), which has been concluded fails in predicting anisotropies in the thermal field [2]. In order to improve numerical predictions, researchers have been working on models focusing on a variable turbulent Prandtl number (Pr_t), based on the available experimental data, in order to achieve better predictions in the potential core, transition region and self-similar region (fully developed region) of a cryogenic nitrogen jet.
Several variable turbulent Prandtl number models available in the literature (both for sub- and supercritical conditions) are tested and compared with available experimental data for validation purposes and applicability to the modeling of LRE combustion chambers at supercritical conditions.

The turbulent Prandtl number
The turbulent Prandtl number is defined as the ratio of eddy diffusivity of momentum (ϵ_m) to eddy diffusivity of heat (ϵ_h), given by equation 1.

$$\mathrm{Pr}_t = \frac{\epsilon_m}{\epsilon_h} \tag{1}$$

In turn, eddy diffusivity of momentum and heat are related to the Reynolds stresses by equations 2 and 3.

$$\overline{u'v'} = -\epsilon_m \frac{\partial u}{\partial y} \tag{2}$$

$$\overline{T'v'} = -\epsilon_h \frac{\partial T}{\partial y} \tag{3}$$

As expressed by [3], knowledge regarding turbulent shear stress and heat flux, velocity, and temperature gradients is required for the turbulent Prandtl number to be evaluated in this regard, that is through equation 4. However, difficulties in the measurements of these quantities make the availability of experimental data scarce and more often than not conflict. The concept of a turbulent Prandtl number is the most often used to close the energy equation, from which temperature gradients are evaluated numerically [4].

$$\mathrm{Pr}_t = \frac{\overline{u'v'}\frac{\partial T}{\partial y}}{\overline{T'v'}\frac{\partial u}{\partial y}} \tag{4}$$

Table 1. Review of variable turbulent Prandtl number models.

Model	Observations
$\mathrm{Pr}_t = 0.75 + \frac{1.63}{\ln\left(1 + \mathrm{Pr}/0.0015\right)}$ (5)	Empirical Pr_t model formulated as a function of Pr. Equations are discretized following a Finite Volume Method (FVM), for steady state conditions, with an improved κ-ϵ turbulence model at the wall. The model is applied to fully developed pipe flow, with the test subject being water [1].
$\mathrm{Pr}_t = 1.855 - \tanh\left[0.2\left(y^+ - 7.5\right)\right].$ (6)	Based on experimental evidence from Laser Doppler Velocimetry (LDV) that Pr_t varies with distance from the wall, being the test subject water. The effect of concave curvature is also studied [4]
$\mathrm{Pr}_t = \left[\frac{1}{7} + \frac{0.3\mathrm{Pe}_t}{\sqrt{0.85}} - \left(0.3\mathrm{Pe}_t\right)^2\left[1 - \exp\left(-\frac{1}{\sqrt{0.85}\left(0.3\mathrm{Pe}_t\right)}\right)\right]\right]^{-1}$ (7)	Tested for air. The model is based on experimental data. For gases, it can only be seen as an empirical fit to the experimental data. The model does not include the effects of pressure gradients [6].
$\mathrm{Pr}_t = \begin{cases} 1.07 & , y^+ \leq 10 \\ \frac{2}{\mathrm{Pe}_t} + 0.85 & , y^+ > 10 \end{cases}$ (8)	The model is applied to flat plate boundary layers with a null pressure gradient and fully developed flow in a tube or pipe. The test subjects are air and water [3].
$\mathrm{Pr}_t = c\left(\frac{\mathrm{Pe}_t}{\mathrm{Re}_t}\right)$ (9)	The computations are performed using the realizable version of the κ-ϵ turbulence model, following Favre averages. This model has the disadvantage of the parameter c being case dependent. The test subject is water at supercritical conditions [7].
$\mathrm{Pr}_t = \begin{cases} 1.0 & , \frac{\mu_t}{\mu} < 0.2 \\ 0.85 + \frac{\mathrm{Pr}}{A} & , 0.2 \leq \frac{\mu_t}{\mu} \leq 10 \\ 0.85 & , 10 < \frac{\mu_t}{\mu} \end{cases}$ (10)	The computations are performed using the κ-ω SST turbulence model, following Favre's averaging procedure. Pressure and velocity are coupled with the SIMPLE algorithm. The model is applied to vertical heat tubes and the test subject is supercritical carbon dioxide [8].

Nevertheless, several attempts at incorporating variable turbulent Prandtl number into numerical modeling, both at sub- and supercritical conditions are documented in the literature. In the work of [5], the challenges related to the modeling of the turbulent Prandtl number are highlighted, and some simple guides in the form of questions, futures models should be able to answer is provided. Even though the author performs a thorough review of the available models, the prediction of departures from the Reynolds analogy is still an open issue. Even though models

may vary in complexity and applicability, common ground can be found between them - turbulent Prandtl's number dependence on molecular Prandtl. This can be seen in the selection of models of Table 1, to be tested for cryogenic nitrogen jets injection.
The model of [1] (equation 5) directly puts in evidence the dependence of Pr_t on Pr with the addition of some empirical constants. The influence of a concave surface on Pr_t is studied by [4] (equation 6), proposing a model dependent on the distance to the wall (y^+), incorporating the behavior of the different regions in the boundary layer. Conventionally, density fluctuations are neglected, and in accord, the use of a constant value for the turbulent Prandtl number allows for compressibility effects to be modeled by mean density alone, in accord to Morkovin's hypothesis.
Some more contributions into the matter arise from the works of [6] (equation 7) and [3] (equation 8). An increased dependent from Pr_t on Pr is incorporated in these models with the inclusion of the turbulent Péclet number. The authors analyze the influence of both laminar and turbulent Prandtl numbers (equation 11) as is commonly used in the closure of the energy equation.

$$\frac{1}{\mathrm{Pr}} + \frac{\epsilon_m/\nu}{\mathrm{Pr_t}} \tag{11}$$

The first term of relation 11 refers to molecular conduction, while the second one to the turbulent one. From here it can be concluded if $\mathrm{Pr} >> 1$, molecular conductivity is negligible, while if $\mathrm{Pr} << 1$ the molecular term can be larger than the turbulent one. This analysis is of particular importance in the modeling of boundary layers.
An entirely different approach is proposed by [9], where it is suggested the abandon of eddy diffusivity concept and consequently of the Boussinesq approach entirely in favor of modeling in terms of wall units.
Modeling through a variable turbulent Prandtl number is also the subject of [10], [11] and [12], on heat transfer deterioration, meaning the incapability in removing of heat at the wall by the fluid flow. The models of [1], [3], [4], and [6] are put to the test, being the most relevant conclusion a decrease in Pr_t due to an increase in the diffusion term of the energy equation, for both heat transfer regimes (deteriorated and normal).
The model of [7], [13] (equation 9) developed for the study of supercritical water jets is based on the ratio between turbulent Péclet and Reynolds number, plus the contribution on an empirical constant. This empirical constant, c is case dependent, a clear disadvantage of the model.
To the best of the authors' knowledge, the first time an attempt is made of using an analytical variable turbulent Prandtl number model on the study of cryogenic nitrogen jet injection if the one of [14], where the model of [7] was tested. It is concluded that even though this model seems promising for applications in supercritical water, it is not suited for simulations with nitrogen, where better results were achieved with a constant value for the turbulent Prandtl number.
The last model considered is the one proposed by [8] (equation 10). In this model, the ratio $\frac{\mu_t}{\mu}$ is used to identify the fully developed turbulence region, the transition and the viscous sublayer, a constant value of 0.85 is used for the fully developed turbulence region, while the value of 1 is used for the viscous sublayer, in accordance to [3]. It is also stated the proportionality between Pr_t and Pr in the transition region. In this model, the influences of the different regions of the boundary layer are modeled, while outside of it, the model resorts to a constant turbulent Prandtl number of 1.
In summary, the numerical studies performed prove that all current turbulence models apply with limiting conditions, [15].

Numerical model
Conservation for mass, momentum and energy in steady state are modeled with Favre averages, equations 12, 13 and 14, respectively.

$$\frac{\partial \overline{\rho}\widetilde{u_i}}{\partial x_i} = 0 \tag{12}$$

$$\frac{\partial \overline{\rho u_i u_j}}{\partial x_j} = -\frac{\partial \overline{p}}{\partial x_i} + \frac{\partial \overline{\tau_{ij}}}{\partial x_j} \tag{13}$$

$$\frac{\partial \overline{\rho}\widetilde{u_j}\widetilde{H}}{\partial x_j} = \frac{\partial \overline{\tau_{ij} u_i}}{\partial x_j} - \frac{\partial \widetilde{u_i}\overline{\rho}\widetilde{u_i'' u_j''}}{\partial x_j} - \frac{\partial (\overline{q_j} + \overline{\rho}\widetilde{u_j'' h''})}{\partial x_j} \tag{14}$$

The standard two equations $\kappa - \epsilon$ turbulence model of [16] is used to account for Reynolds stresses, through Boussinesq's approach (equation 15).

$$\tau_{ij} = 2\mu_t \left(S_{ij} - \frac{1}{3}\frac{\partial u_k}{\partial x_k} \right) - \frac{2}{3}\rho k \delta_{ij} \tag{15}$$

The real gas equation of state of Soave-Redlich-Kwong [17] is used to close the system and to account for high-pressure effects. On the other hand, transport properties such as thermal conductivity and dynamic viscosity are

evaluated through [18]. These properties are expressed as the sum of ideal-gas conditions, and departure functions are used, taking into account dense fluid corrections.
The resulting system of equations is then discretized following a Finite Volume/ Finite Difference Method with the QUICK scheme of Leonard [19] used to account for numerical diffusion. A second-order central scheme is used up to the point where advection transport rate is twice that of diffusion, meaning the Péclet number (Pe) is 2. At this point, the first order upwind scheme is used. The introduced numerical diffusion is then treated with the QUICK scheme. The SIMPLE [20] algorithm is employed for pressure coupling, and the resulting algebraic equations are solved following a line by line application of the Thomas Tridiagonal Matrix Algorithm until convergence is reached.

Results and discussion
The experimental work of [21] is used for validation of the injection of a nitrogen jet into a combustion chamber. More specifically cases 3 and 4 are simulated. Injection and chamber conditions are summarized on Table 2.

Table 2. conditions for cases 3 and 4, [21].

Condition	Transcritical (case 3)	Supercritical (case 4)
Chamber temperature T_∞ [K]	298	298
Chamber pressure p_∞ [MPa]	3.97	3.98
Injection temperature T_0 [K]	126.9	137
Injection velocity v_0 [m/s]	4.9	5.4
Injection densityρ_0 $[\mathrm{kg/m^3}]$	435	171
Chamber density ρ_∞ $[\mathrm{kg/m^3}]$	45.5	45.5

The north boundary is set as a constant temperature wall, while the west boundary is an adiabatic wall. The south wall corresponds to the symmetry axis, as only half of the chamber is simulated and the east wall is the outlet. The injector has an inner diameter of 2.2 mm; the computational domain is 250 mm long and 122 mm wide. The boundary conditions and the test geometry are presented in Figure 1.

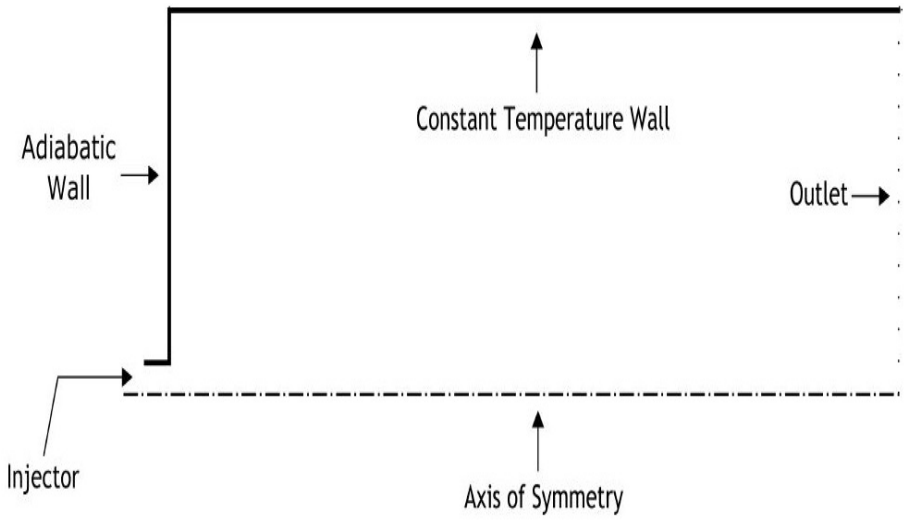

Figure 1. Boundary conditions and test geometry.

Figure 2 depicts the results for the center-line axial density distribution for the transcritical case. In the horizontal axis, the distance from the injector is normalized by the injector's diameter, while in the vertical axis, the density evolution is displayed. The variable turbulent Prandtl number models of Table 1, are compared with three computations with a constant turbulent Prandtl number of 0.6, 0.8 and 1. The results are compared with the experimental data of [21] for validation purposes and with the Large Eddy Simulation (LES) from [22] and [23]. From the Figure, it can be seen all models, agree in the potential core of the jet (up until X/D=12), except the LES ones. The value in center-line density of 400 $\mathrm{kg/m^3}$ corresponds to the actual value measured by [21] for this case. Since all models tested do show the same evolution of center-line density in the potential core, it can be concluded, the turbulent Prandtl number has a negligible effect in this region. The fact the models lead to a denser potential core than what was predicted experimentally can be related to the peak in specific heat characteristic of the critical point. Following the conclusions of [14], though the model of [7] has some interesting results for water, it is not useful for nitrogen. The models of [1], [8] and the constant value computations (the line of $\mathrm{Pr}_t = 1$ and the model of [8] overlap each other) translate the effect of a rapid transfer of momentum and thermal energy, into the fully developed turbulent region where the models seem to converge.
Overall, the computations seem to indicate the use of a variable turbulent Prandtl number model is of particular importance in the transition region of the jet.

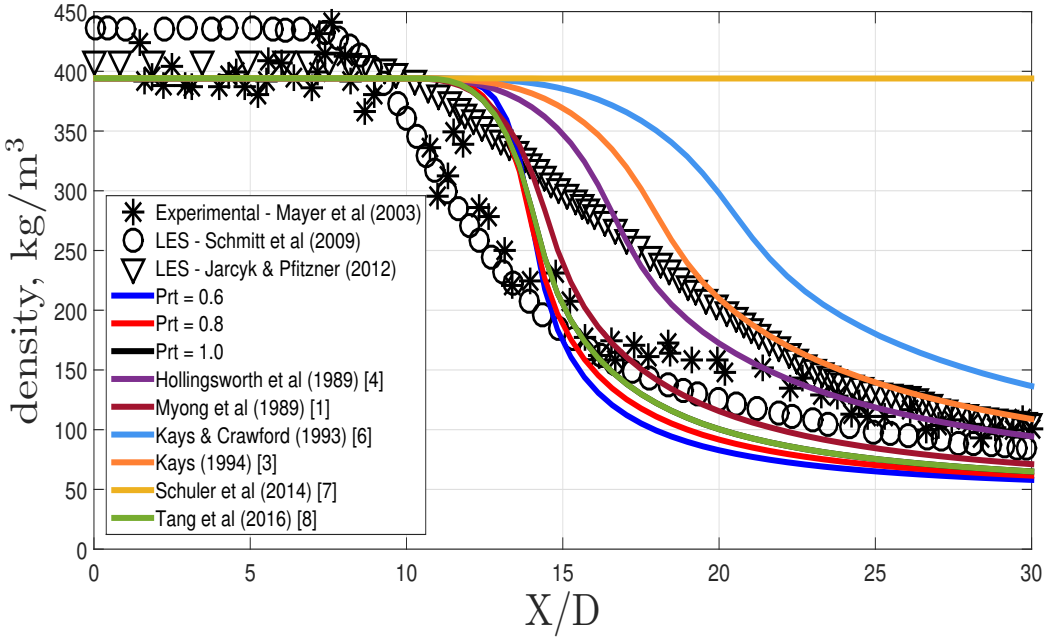

Figure 2. Center-line axial density distribution for the transcritical case.

The evolution of a jet from the nozzle's discharge until a self-similar solution is reached displayed in Figure 3.

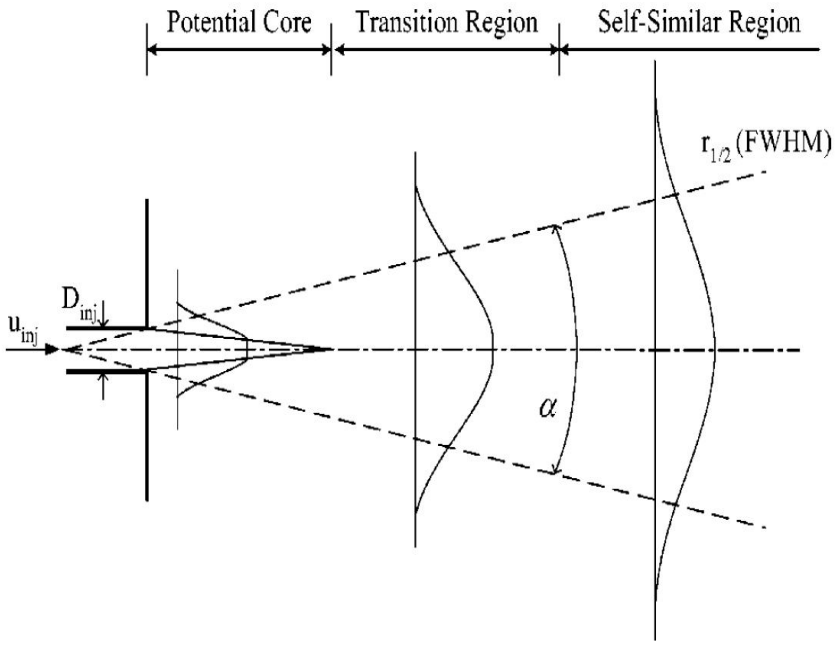

Figure 3. Jet constitution,[24].

In Figure 4 the results concerning the Full Width at Half Maximum (FWHM) of density are presented. It represents the difference between the maximum and minimum of an independent variable at which the dependent variable is equal to half its maximum value. Overall the experimental data is better approximated by the model of [4] capable of predicting jet warming and dissipation. The models of [6] and [3] are only capable of an accurate prediction until $\mathrm{X/D} = 15$. The model by [8] which correlated fairly well with experimental data in the center-line axial density distribution (Figure 2) fails in the prediction of the FWHM of density for the transcritical case.
Regarding the supercritical conditions at which the models were evaluated, it can be seen in Figure 5 a similar trend to transcritical conditions, in the sense all models produce the same results in the potential core (in this case, the difference in terms of the core size between computational and experimental results is smaller than the one obtained for transcritical conditions). The model by [7] continues to fail in predicting any variation. The models by [1],[4], [8]

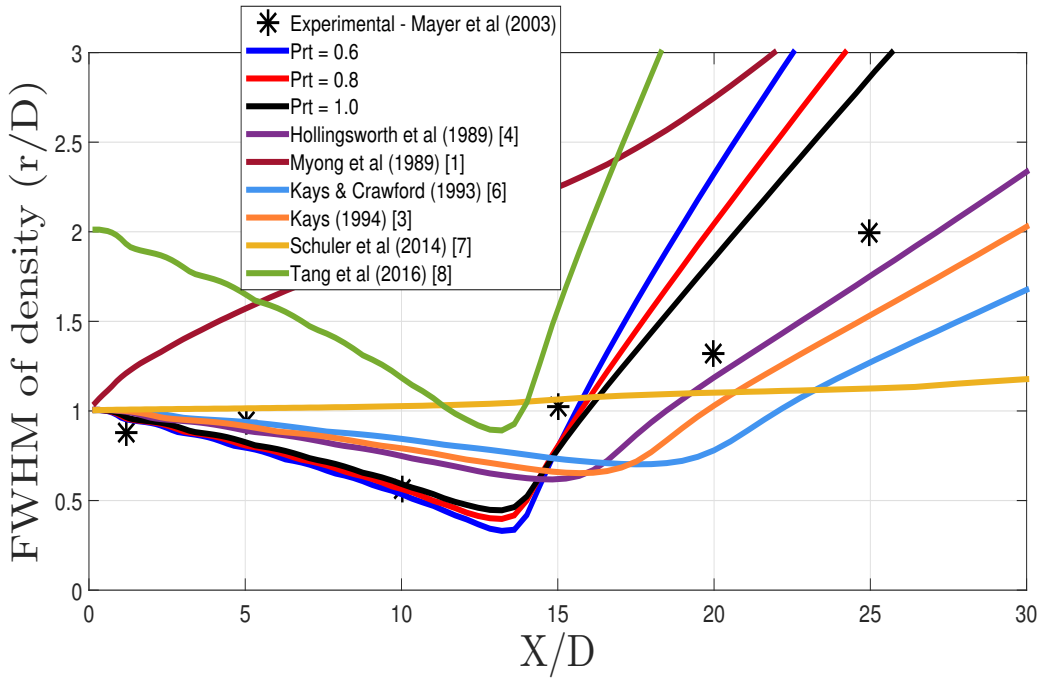

Figure 4. Full Width at Half Maximum of density for the transcritical case.

and the constant turbulent Prandtl number show the same trend as the self-similar region is approached.

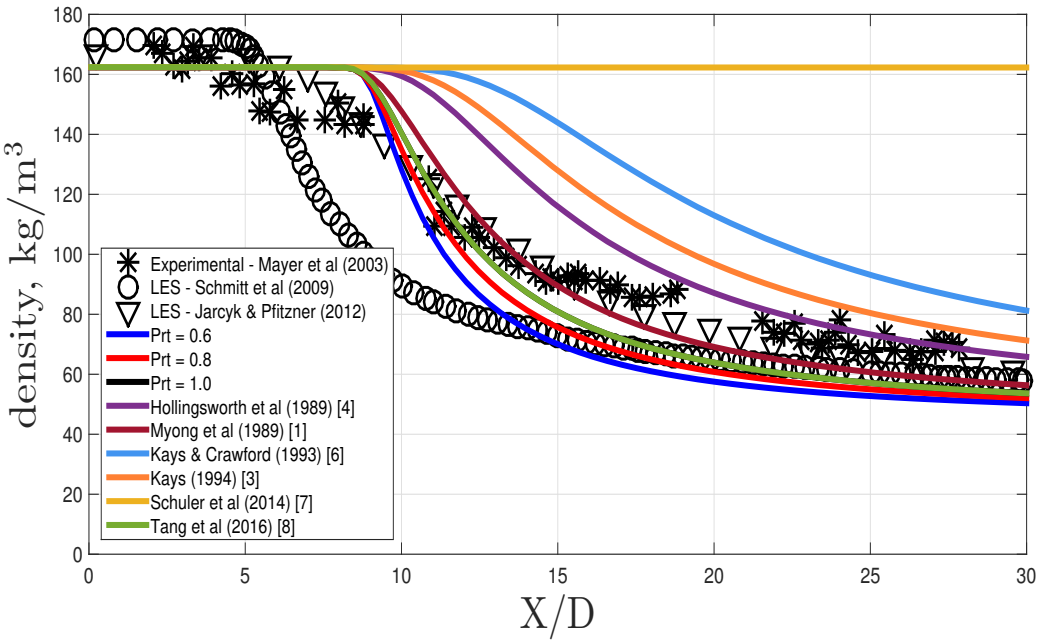

Figure 5. Center-line axial density distribution for the supercritical case.

From the overall analysis of the results, it can be seen at both transcritical and supercritical conditions, the potential core of the jet is not affected by the different turbulent Prandtl number models (either constant or variable), and the present computations are in better agreement with the experimental data than the Les simulations of [22] and [23], except at the end of the core, where LES computations predict a shorter one. In the transition region, considerable differences between present models can be seen. It is in this region the modeling of a turbulent Prandtl number has a considerable effect, effectively determining the way the jet approaches the fully developed region. It is also possible to observe concerning the present computations the same level of agreement with experimental data is reached, either for transcritical or supercritical conditions, which does not happen when compared to the works of [22] and [23].

As a result, the present is a successful contribution to the understanding of nitrogen cryogenic nitrogen injection

phenomena at transcritical and supercritical conditions. However, work has yet to be done to understand if present conclusions are a result of the turbulence model used or if they represent a more general trend.

Conclusions

Overall the numerical results obtained correlate well with the available experimental data. The potential core seems to be the least affected region of the jet, allowing for the conclusion, the effect of the turbulent Prandtl number is negligible in this region. On the other hand, the models start to evolve into a self-similar solution around $\mathrm{X/D} = 25$. The transition region is the one where more efficiency in the modeling of the turbulent Prandtl number is needed, shown through the various results obtained in center-line axial density distribution by using the different models.
Further validation of the models is required in nitrogen jets injection at transcritical and supercritical conditions to assess if the obtained results are a characteristic of these specific conditions or illustrate a more general trend. Lastly, the same analysis can be made regarding the turbulence model used.

Acknowledgements

The present work was performed under the scope of Aeronautics and Astronautics Research Center (AeroG) of the Laboratório Associado em Energia, Transportes e Aeronáutica (LAETA) activities and it was supported by Fundação para a Ciência e Tecnologia (FCT) through grant number SFRH/BD/136381/2018 an project number UID/EMS/50022/2019.

Nomenclature

FWHM	Full Width at Half Maximum
FVM	Finite Volume Method
LES	Large Eddy Simulation
LRE	Liquid Rocket Engine
SRK	Soave Redlich Kwong
QUICK	Quadratic Interpolation for Convective Kinematics
SIMPLE	Semi-Implicit Method for Pressure Linked Equations
SST	Shear Stress Transport
Pr	Prandtl number
Pr_t	turbulent Prandtl number
Pe	Péclet number
Pe_t	turbulent Péclet number
Re_t	turbulent Reynolds number
$A = 15$	model constant
$c = 3.5$	model constant
p_∞	chamber pressure [MPa]
T_0	injection temperature [K]
T_∞	chamber temperature [K]
v_0	injection velocity [m/s]
ρ_0	injection density [kg/m^3]
ρ_∞	chamber density [kg/m^3]
κ	turbulent kinetic energy
ϵ	turbulent kinetic energy dissipation
ϵ_m	eddy diffusivity of momentum
ϵ_h	eddy diffusivity of heat
ω	specific turbulent kinetic energy dissipation
ν	Kinematic viscosity [Pa.s]
y^+	distance from the wall

References

[1] H. Myong and N. Kasagi and M. Hirata, 1989, *JSME International Journal*, 32 (4), pp. 613-622.
[2] M. Aouissi and A. Bounif and K. Bensayah, 2008, *Heat and Mass Transfer*, 44 (9), pp. 1065-1077.
[3] W. M. Kays, 1994, *Journal of Heat Transfer*, 116 (2), pp. 284-296.
[4] D. K. Hollingsworth and R. J. Moffat and W. M. Kays, 1992, *Experimental Thermal and Fluid Science*, 5 (3), pp. 299-306.
[5] A. J. Reynolds, 1975, *International Journal of Heat and Mass Transfer*, 18 (9), pp. 1055-1069.
[6] W. M. Kays and M. E. Crawford, 1993, "Convective heat and mass transfer", 3rd Edition, McGraw Hill, New York.
[7] M. J. Schuler and T. Rothenfluh and P. Stathopoulos and D. Brkic and T. Meier and P. R. von Rohr, 2014, *Chemical Engineering & Technology*, 37 (11), pp. 1896-1902.
[8] G. Tang and H. Shi and Y. Wu and J. Lu and Z. Li and Q. Liu and H. Zhang, 2016, *International Journal of Heat and Mass Transfer*, 102, pp. 1082-1092.
[9] S. W. Churchill, 2002, *Industrial & Engineering Chemistry Research*, 41 (25), pp. 6393-6401.

[10] M. Mohseni and M. Bazargan, 2011, *Journal of Heat Transfer*, 133 (7), pp. 1-10.
[11] M. Mohseni and M. Bazargan, 2016 *Journal of Heat Transfer*, 138 (8), pp. 1-9.
[12] Z. Wang and P. Jiang and R. Xu, 2018 *Heat Transfer Engineering*, pp. 1-11.
[13] M. J. Schuler and T. Rothenfluh and P. R. von Rohr, 2013, *The Journal of Supercritical Fluids*, 75, pp. 128-137.
[14] J. Sierra-Pallares and J. Garcia del Valle and P. Garcia-Carrascal and F. Castro Ruiz, 2016, *The Journal of Supercritical Fluids*, 115, pp. 86-98.
[15] Y. Bae, 2016 *International Journal of Heat and Mass Transfer*, 92, pp. 792-806.
[16] K. Chien, 1982 *AIAA Journal*, 20 (1), pp.33-38
[17] G. Soave, 1972, *Chemical Engineering Science*, 27 (6), pp. 1197-1203.
[18] E. W. Lemmon and R. T. Jacobsen, 2004, *International Journal of Thermophysics*, 25 (1), pp. 21-69.
[19] B. P. Leonard, 1979 *Computer Methods in Applied Mechanics and Engineering*, pp.58-98
[20] S. V. Patankar, 1972, "Numerical heat transfer and fluid flow", Hemisphere Publishing Company.
[21] W. Mayer and J. Telaar and R. Branam and G. Schneider and J. Hussong, 2003 *Journal of Heat and Mass Transfer*, 39 (8-9), pp. 709-719.
[22] T. Schmitt and L. Selle and B. Cuenot and T. Poinsot, 2009, 337 (6-7), pp. 528-538.
[23] M. Jarczyk and M. Pfitzner, Jan. 9.-12. 2012, 50th AIAA Aerospace Sciences Meeting including the New Horizons Forum and Aerospace Exposition.
[24] N. Zong and H. Meng and S. Hsieh and V. Yang, 2004, *Physics of Fluids*, 16 (12), pp. 4248-4261.